PUBLICATIONS OF THE ASTRONOMICAL SOCIETY OF THE PACIFIC, **118**:288–296, 2006 February

The Automatic Real-Time Gamma-Ray Burst Pipeline of the 2 m Liverpool Telescope

C. GUIDORZI,[1] A. MONFARDINI,[2] A. GOMBOC,[1,3] C. J. MOTTRAM, C. G. MUNDELL,[4] I. A. STEELE, D. CARTER, M. F. BODE,[5] R. J. SMITH, S. N. FRASER, M. J. BURGDORF, AND A. M. NEWSAM

Astrophysics Research Institute, Liverpool John Moores University, Twelve Quays House, Birkenhead CH41 1LD, UK; crg@astro.livjm.ac.uk

Received 2005 August 25; accepted 2005 October 31; published 2006 February 9

ABSTRACT. The 2 m Liverpool Telescope (LT), owned by Liverpool John Moores University, is located in La Palma (Canary Islands) and operates in fully robotic mode. In 2005, the LT began conducting an automatic gamma-ray burst (GRB) follow-up program. On receiving an automatic GRB alert from a gamma-ray observatory (*Swift*, *INTEGRAL*, *HETE-2*, or IPN), the LT initiates a special override mode that conducts follow-up observations within 2–3 minutes of the GRB onset. This follow-up procedure begins with an initial sequence of short (10 s) exposures acquired through an r' band filter. These images are reduced, analyzed, and interpreted automatically using pipeline software developed by our team, called LT-TRAP (Liverpool Telescope Transient Rapid Analysis Pipeline); the automatic detection and successful identification of an unknown and potentially fading optical transient triggers a subsequent multicolor imaging sequence. In the case of a candidate brighter than $r' = 15$, either a polarimetric (from 2006) or a spectroscopic observation (from 2007) will be triggered on the LT. If no candidate is identified, the telescope continues to obtain z', r', and i' band imaging with increasingly longer exposure times. Here we present a detailed description of the LT-TRAP and briefly discuss the illustrative case of the afterglow of GRB 050502a, whose automatic identification by the LT just 3 minutes after the GRB led to the acquisition of the first early-time (<1 hr) multicolor light curve of a GRB afterglow.

1. INTRODUCTION

Since the discovery of the first optical afterglow (van Paradijs et al. 1997) associated with a gamma-ray burst (GRB), several robotic telescopes have been developed to perform rapid follow-up observations of GRB afterglows. Fast robotic follow-ups are now possible because of the improved localization of GRBs provided by current gamma-ray satellites (*HETE-2*, *INTEGRAL*, *Swift*, and the Interplanetary Network); real-time GRB alerts are received from these satellites through the GRB Coordinates Network (GCN)[6] within a few seconds of the GRB onset and provide positions with typical uncertainties of a few arcminutes. Observations within minutes of the GRB can be crucial to determine the properties of the close circumburst environment, potentially providing clues to the nature of the progenitor.

To date, there are only a few GRBs for which we have measurements of optical afterglow starting as early as a few minutes after the GRB: 990123, 021004, 021211, 030418, 041006, 041218, 041219a, 050319, 050401, 050502a, 050525, 050712, 050713A, 050730, 050801, 050802, 050820A, 050824, 050904, 050908, 050922C, and 051021A (2005 October). Figure 1 shows the early afterglow light curves for all of them within the first day after the burst. For each GRB, we collected unfiltered R, R_C, and V observations.

2. THE LIVERPOOL TELESCOPE

The Liverpool Telescope (LT), owned and operated by Liverpool John Moores University (LJMU), has a 2 m diameter primary mirror, an altitude-azimuth design, and a final focal ratio of f/10. It was designed and built by Telescope Technologies Limited, with the robotic control system and instrumentation being provided by the LJMU Astrophysics Research Institute (Steele et al. 2004). It is situated at the Observatorio del Roque de los Muchachos, on the Canary Island of La Palma. Due to the fully opening enclosure and the fast slew rate of $2^\circ\ s^{-1}$, the telescope can start observations within 1–3 minutes of receipt of the GCN alert notice. LT has five instrument ports (four folded and one straight-through), selected by a deployable rotating mirror in the AG (aquisition and guidance) box within 30 s. The telescope is equipped with the RATCam optical CCD camera and the SupIRCam 1–2.5 μm camera.

A prototype spectrograph and an optical polarimeter (RINGO) based on a design by Clarke & Neumayer (2002) are expected to be operating later in 2006. A higher resolution,

[1] Marie Curie Fellow.

[2] Current address: ITC–IRST and INFN, Trento, Via Sommarive 18, 38050 Povo (TN), Italy.

[3] Current address: FMF, University in Ljubljana, Jadranska 19, 1000 Ljubljana, Slovenia.

[4] Royal Society University Research Fellow.

[5] PPARC Senior Fellow.

[6] See http://gcn.gsfc.nasa.gov/gcn (S. Barthelmy et al. 2005).

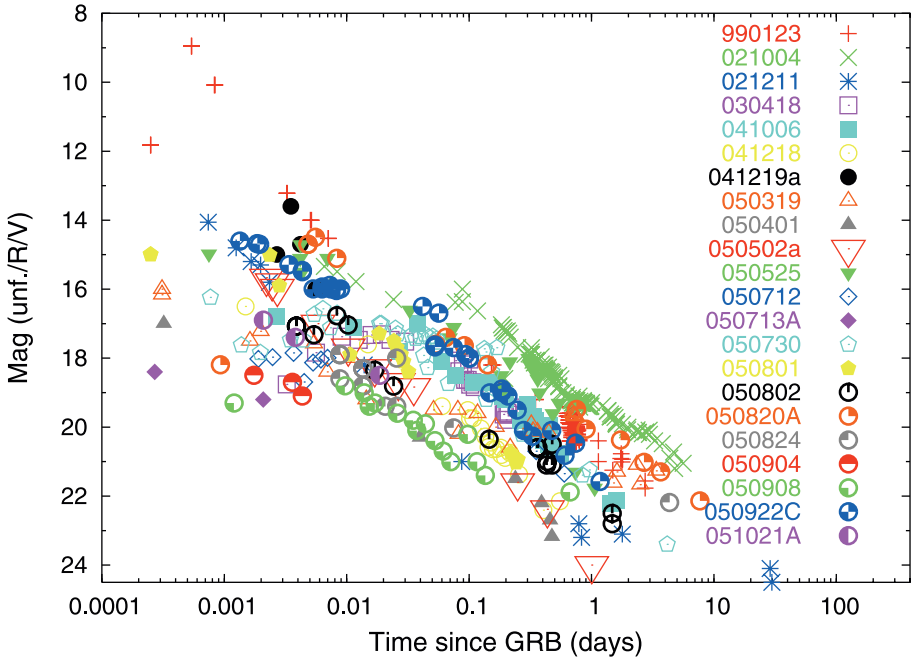

FIG. 1.—Early light curves (unfiltered, *R* and *V*) for a set of GRBs with detections within minutes of the gamma-ray event. Big open inverted triangles show the case of GRB 050502a (filter *r*′) robotically detected and followed-up by LT (from Guidorzi et al. 2005a). All the measurements shown have been taken from GCN Circulars (Nos. 248, 257, 307, 715, 1572, 1589, 1596, 1732, 1738, 1739, 1748, 1752, 1759, 1821, 2773, 2776, 2784, 2798, 2799, 2821, 2875, 2897, 3118, 3165, 3480, 3485, 3487, 3489, 3492, 3575, 3584, 3588, 3596, 3601, 3604, 3646, 3704, 3705, 3711, 3712, 3716, 3717, 3718, 3720, 3723, 3726, 3728, 3733, 3736, 3739, 3741, 3744, 3745, 3746, 3756, 3765, 3775, 3778, 3829, 3834, 3836, 3838, 3853, 3863, 3864, 3865, 3868, 3869, 3870, 3880, 3883, 3896, 3907, 3917, 3929, 3943, 3944, 3945, 3947, 3950, 3953, 3960, 4011, 4012, 4015, 4016, 4018, 4023, 4026, 4027, 4032, 4041, 4044, 4046, 4048, 4049, 4095, 4120, and 4121), except for GRB 030418 (Rykoff et al. 2004), GRB 041219a (Vestrand et al. 2005), and GRB 050502a (Guidorzi et al. 2005a).

higher sensitivity, and generally more capable spectrograph (FRODOSpec) is being developed for deployment in 2007. Table 1 reports the main characteristics of each instrument. In addition to the GRB follow-up program, which has high priority on the LT, the robotic control (Fraser & Steele 2002) and automated scheduler (Steele & Carter 1997; Fraser & Steele 2004) allow the LT to conduct an optimized science program of observations of time variable sources over a wide range of timescales from targets of opportunity (e.g., novae, supernovae, and anomalies in gravitational lenses) to longer term monitoring (e.g., AGNs, variable stars) when no GRB observations are required.

3. REAL-TIME GRB FOLLOW-UP STRATEGY: OVERVIEW

When a GRB fulfills all the requirements to be observed with the LT, the GRB override mode is triggered. The GRB program takes control of the telescope and triggers the so-called detection mode (§ 5), during which a small number of Sloan

TABLE 1
LIVERPOOL TELESCOPE INSTRUMENTATION

Instrument	Description
RATCam optical CCD camera	2048 × 2048 pixels, 0.″135 pixel^{-1}, FOV 4.′6 × 4.′6, eight filter selections (u′, *g*′, *r*′, *i*′, *z*′, *B*, *V*, Hα, ND 2.0) (from LT first light, 2003 July)
SupIRCam 1–2.5 μm camera (with Imperial College)	256 × 256 pixels, 0.″4 pixel^{-1}, FOV 1.′7 × 1.′7; *Z*, *J*, *H*, *K*′ filters (from late 2005)
Prototype spectrograph (with University of Manchester)	49 1.″7 fibers, 512 × 512 pixels, $R = 1000$; 3500 Å < λ < 7000 Å (starting in 2006)
RINGO optical polarimeter	Ring polarimeter based on the design of Clarke & Neumayer (2002), starting in 2006
FRODOSpec integral-field double-beam spectrograph (with University of Southampton)	$R = 4000$, 8000; 4000 Å < λ < 9500 Å (starting in 2007)

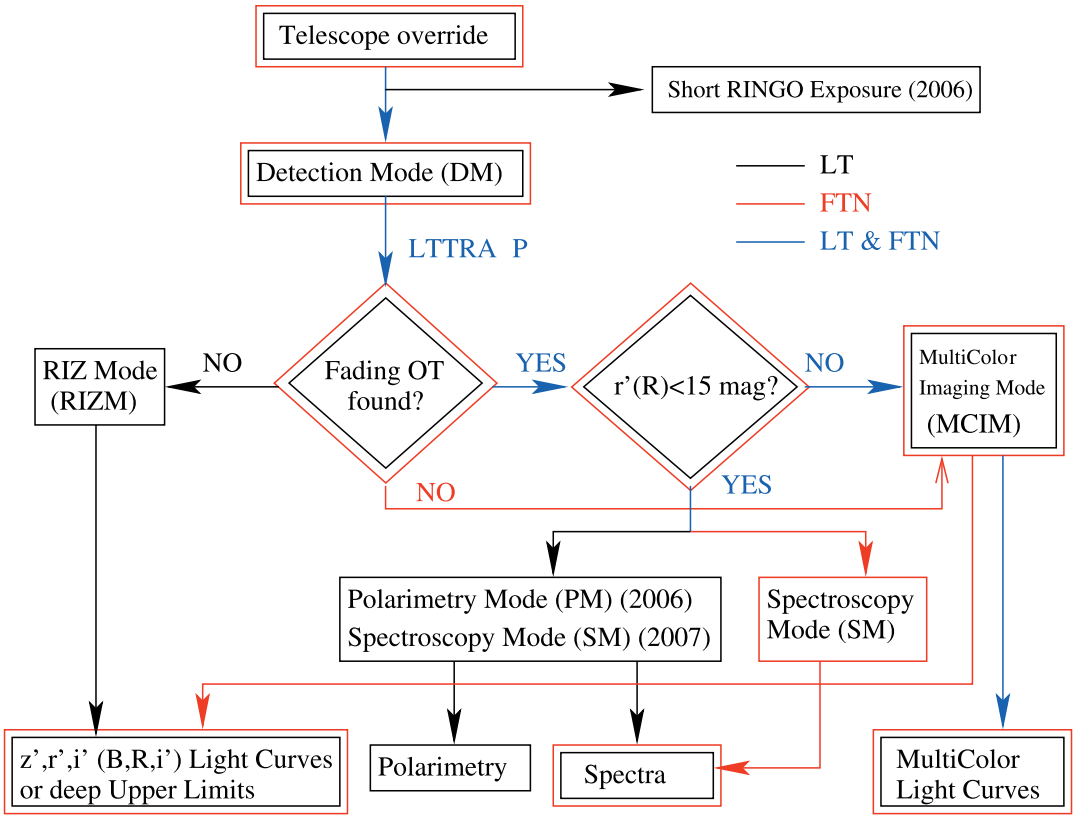

FIG. 2.—Diagram of the LT-TRAP observing strategy for both the LT and FTN facilities.

r'-band short-exposure images are taken.[7] These images are then transferred to the LT proxy machine, a network-attached on-site computer. The automatic LT GRB pipeline, called the Liverpool Telescope Transient Rapid Analysis Pipeline (hereafter LT-TRAP), is then invoked to process, analyze, and interpret these images, and returns a value to indicate whether any variable optical transient (OT) candidate has been identified. The result of this analysis drives the automatic selection of the subsequent observing mode as follows:

1. Identification of a fading OT with $r' > 15 \rightarrow$ multicolor imaging mode (§ 6.1);
2. Identification of a fading OT with $r' \leq 15 \rightarrow$ polarimetry mode (2006) or spectroscopy mode (2007) (§ 6.3);
3. No identification of an OT $\rightarrow$ RIZ mode (§ 6.4).

Figure 2 shows a diagram of the overall observing strategy when the GRB override mode is triggered.

[7] From 2006, this detection mode will be preceded by a short 30 s exposure taken with the RINGO polarimeter.

4. LT GRB OVERRIDE MODE

The GRB Target of Opportunity Control Agent (GRB TOCA) is a shell script that is invoked in response to a GRB alert being received at LT via a socket connection. This script uses the TOCA of the LT Robotic Control System (RCS) to take control of the telescope, provided that the GRB position is observable and that other requirements are fulfilled, e.g.:

1. The positional error circle is sufficiently small (error radius $<10'$).
2. The altitude above the horizon is $>20°$.
3. The position does not match any known X-ray catalog source.
4. In the case of a *Swift* alert, the image significance should not be low (to date, no real GRB has been found to have raised the low image significance flag).
5. None of the five known soft gamma repeaters (SGR 1900+14, SGR 1806−20, SGR 1627−41, SGR 0526−66, and SGR 1801−23) lies in the error circle.

As noted above, the average delay between the arrival time of the GCN alert and the start time of observations ranges between 1 and 3 minutes.

In the case of an SGR lying in the error circle, the GRB TOCA triggers an SGR follow-up IR observation with the SupIRCam, according to the strategy defined in an approved SGR follow-up proposal led by the LT GRB group. Currently, the automatic SGR follow-up program is still being tested, so the presence of an SGR in the error circle merely invalidates the GRB follow-up observation.

When all of the above conditions are fulfilled, the GRB TOCA repoints the telescope and then triggers the acquisition of the first set of images scheduled in the detection mode (following commissioning of RINGO [2006], the detection mode exposures will be preceded by an initial short polarimetric exposure). LT-TRAP is then invoked to analyze these images and consequently choose the most suitable observing strategy (see § 5 for a detailed description). The RINGO exposure will be analyzed offline at a later time and plays no part in real-time decision making; the motivations of this choice are explained in § 6.2.

The GRB TOCA and the LT-TRAP communicate through the notice board, which is a plain-text file that is continuously updated until the end of observations. This not only reports in real time a detailed chronological sequence of all the actions and results acquired, following technical conventions, but also represents a useful real-time human-readable interface for the users responsible for monitoring the ongoing observation sequence.

5. DETECTION MODE (DM)

The DM consists of a sequence of two sets of three 10 s exposure images taken in r'. These are the first images of the GRB field acquired by the telescope. Once each set has been acquired and copied to the proxy machine, the GRB TOCA invokes the GRB astrometric fit script on each image. After object extraction and comparison with standard catalogs, an OT candidates list is created for each set of three images. These OT candidates are then processed by the GRB variability script, which aims to identify sources that are common to each image set and evaluate possible variability. Finally, the DM reports the best OT candidate (if any) out of the two merged lists.

5.1. The GRB Pipeline Astrometric Fit Script

This shell script is responsible for fitting the astrometry and identifying possible OT candidates. Below, we report the detailed sequence of operations performed on each image by this script:

1. Source extraction using a customized version of SExtractor 2.3.2 (Bertin 1996) is performed; if the number of sources extracted is lower than three, it does not attempt to fit the astrometry. In contrast, if more than 20 sources are extracted, only the 20 brightest ones are used in the astrometric fit procedure.

2. A $9' \times 9'$ portion of the USNO-B1.0 astrometric catalog (Monet et al. 2003) centered on the centroid position of the GRB is retrieved from a complete copy stored locally on the LT proxy machine. In case of problems accessing the local catalog, the script attempts to retrieve it through the online interface of the USNO-B1.0.[8]

3. The retrieved catalog image is then cropped to match exactly the field of view of the LT.

4. Optical extinction for the field is determined from the dust maps in Schlegel et al. (1998).

5. An astrometric fit is performed using an adapted version of the WCS (world coordinate system; Greisen & Calabretta 2002) tool `imwcs 3.5.3` (Mink 2002). The fit is considered to have failed if either the number of matched sources is lower than three or if the fraction of matched sources is lower than 50%.

6. If the astrometric fit is successful, the transformation from pixel to sky coordinates is performed with the WCS tool `xy2sky 3.5.7` (Mink 2002), based on the results of the astrometric fit. A typical value for the fit residual is $\sim 0\farcs3$.

7. In the case of astrometric fit failure, all the image sources are in principle considered as potential OT candidates, and they are reported in the OT candidates files, although with a lower confidence level (see below). The pixel-to-sky coordinates transformation is performed assuming the nominal pointing (typical accuracy currently $\sim 10''$–$20''$, with a target of $2''$ on completion of telescope commissioning). In this case, the script ends at this point.

8. Selection of the OT candidates: if the astrometric fit is successful, all the image sources are cross-checked with the catalog stars and classified according to a set of criteria. A 17 bit variable is assigned to each source and describes its properties. Each image source not associated with any USNO-B1.0 star is assigned 50 points. Each bit of the 17 bit variable is assigned a given number of points to be added to the initial 50 point credit (see Table 2).

9. Selected classes of nonassociated image sources are a priori excluded from the candidate search. Among them, the objects with clearly nonstellar point-spread functions (PSFs) are probably the most important (e.g., cosmic-ray events, reflections, and failed deblending). A mean stellar PSF is defined on each image, based on the median statistics of real-time associated objects.

10. Each selected OT candidate is assigned a confidence level directly related to the total number of points accrued.

11. Each selected OT candidate is cross-checked with the online GSC 2.3 (Guide Star Catalog, ver. 2.3) and 2MASS (Two Micron All Sky Survey) catalogs, and its confidence level is adjusted accordingly (see Table 2).

When the astrometric fit is successful, magnitudes are estimated from the USNO-B1.0 stars that have been matched. We use as a zero point the median value of the offset needed to

[8] See http://www.nofs.navy.mil/data/fchpix.

TABLE 2
LT-TRAP : 17 bit Variable Assigned to Each OT Candidate

Bit n	2^{n-1}	Description	Script	Points
1	1	The extracted magnitude is biased by bright neighbors	Astrometric	0
2	2	The object has been deblended	Astrometric	−10
3	4	At least 1 pixel is saturated (>60,000 counts)	Astrometric	0
4	8	Object truncated (close to the image border)	Astrometric	−50
5	16	Aperture data incomplete or corrupted	Astrometric	−10
6	32	Isophotal data incomplete or corrupted	Astrometric	−10
7	64	Memory overflow occurred during deblending	Astrometric	−10
8	128	Memory overflow during extraction	Astrometric	−20
9	256	Was not possible to check GSC and/or 2MASS	Astrometric	−20
10	512	A GSC 2.3 object lies close (<2″)	Astrometric	−50
11	1024	A 2MASS object lies close (<2″)	Astrometric	−30
12	2048	A bright USNO star ($R < 13$) is close (<50 pixels)	Astrometric	−20
13	4096	Astrometric fit failed, assuming nominal pointing	Astrometric	−50
14	8192	Object detected in at least two OT lists	Variability	+30
15	16384	Object not detected in at least one OT list	Variability	−10
16	32768	Variability detected over two to three images	Variability	+50
17	65536	Astrometric fit warning	Variability	0

have a match between the instrumental magnitude and the R magnitude reported in the USNO-B1.0 catalog. The error associated with the zero point is then evaluated in terms of the clipped (2 σ) rms deviation with respect to the USNO-B1.0.

5.2. The GRB Pipeline Variability Script

After the LT-TRAP script described above has run on the three images, the three resulting OT candidates' files, each reporting a list of potential OTs found in each image, are cross-checked through the so-called variability script. This shell script is invoked by the GRB TOCA and aims to recognize objects that are common to each of the OT candidates' files, as well as to evaluate possible significant magnitude variations between the three images. This variation is evaluated by performing a χ^2 test on the null hypothesis that there is no significant variation. If the three values of magnitude are found to be consistent, with a constant value showing a significance lower than 1%, the variability bit is raised (Table 2). Each OT candidate confidence level is finally adjusted on the basis of the variability results (bit number 16; see Table 2).

Table 2 reports the meaning of each bit of the 17 bit variable assigned to each OT candidate and the points assigned to each flag. The confidence level is evaluated by dividing the total points by 100: when this ratio is <0, the confidence level is set to zero; when the ratio is >1, the level is assigned 1.0 (highest possible confidence level). The final threshold on the confidence level for an OT candidate to trigger the multicolor imaging mode (§ 6.1) is currently set at 0.7. In the case of more than one OT candidate with a confidence level above the threshold, the GRB TOCA accepts the candidate with the highest value. If the ambiguity is still unresolved, it accepts the first on the list. However, all the information regarding the other candidates is reported in the notice board file, as well as in the product files.

The meaning of each single bit described in Table 2 is self-explanatory, except for the last bit, called the "astrometric fit warning," which requires an explanation. This bit is raised whenever at least one of the three images has a failure in the astrometric fit and at least another one has a successful astrometric fit. In this case, the identification of the same object in different images is performed on the basis of pixel coordinates, while the sky coordinates are taken from the image with the correct astrometry. However, so far this case has turned out to be very rare: either all or none of them are successfully astrometrically fitted. For this reason, the current points assigned to this bit are zero.

To test the sensitivity of the script, we simulated an OT fading on real images, according to a power law $F \propto (t - t_0)^{-\alpha}$ (where t_0 is the GRB onset time). The script detected significant variability for $\alpha \sim 1$–2 for objects at least as bright as $r' \simeq 16$–17, provided that the DM is triggered at $t - t_0 < 200$ s. In addition, in the case of GRB 050502a, where the DM was triggered at $t - t_0 = 187$ s, the LT-TRAP detected significant variability: the magnitudes evaluated by the LT-TRAP were for the three DM images ($r'_1 = 15.57 \pm 0.03$, $r'_2 = 15.66 \pm 0.03$, and $r'_3 = 15.83 \pm 0.03$). The corresponding χ^2 test gave the result $\chi^2/\mathrm{dof} = 36.2/2$, with a significance of 1.4×10^{-8}.

It must be pointed out that the systematic error affecting the USNO-B1.0 magnitudes is around 0.3 mag; furthermore, it is not possible to correct for color terms at this stage. However, this is not relevant, as the purpose of the script is to establish relative variations, regardless of the absolute values. To account for possible variations in the zero point, the script adopts the following approach: it calculates the rms deviation of the three zero points and adds it in quadrature to the statistical error of each of the three magnitudes.

6. OBSERVATION MODES

After the DM has completed its imaging and analysis sequence, the appropriate observation mode is triggered auto-

TABLE 3
LT-TRAP Strategy: Observing Modes for Different Facilities

Observing Mode	Liverpool Telescope	Faulkes Telescope North
DM	2 × (3 × 10 s in r')	(3 × 10 s in R) + (1 × 10 s in B, V, i')
RIZM[a]	(n × 2 minutes) in (r', i', z')[a], n = 1, 2, 3, …	…
MCIM	2 × (30 s in g', r', i') + n × (1 minute in g', r', i')	Cycles of B, R, i': 1 × 30 s, 1 × 1 minute, n × (2 minutes, 3 minutes)
SM	For OTs with $r' < 15$ mag (expected in 2007)	$R < 15$ mag
PM	30, 60, 120 s … for OTs with $r' < 15$ mag (2006)	…

[a] Original RIM amended to RIZM by inserting additional z' exposures at the end of each $r'i'$ cycle (from 2005 November).

matically on the basis of the results of the analysis performed by the LT-TRAP on the DM images (see Fig. 2 and Table 3).

6.1. Multicolor Imaging Mode (MCIM)

This mode is triggered by the GRB TOCA when the DM finds an OT candidate with the required confidence level. It consists of a multicolor imaging sequence cycling through three Sloan filters (g', i', and r') until the end of the first hour. The ordered sequence, $g'i'r'$, is repeated with different exposure times: the first two times with 30 s exposures, then continuing with 60 s exposure cycles, up to 18 times. Before 2005 May 16, this mode operated in the same way but used a slightly different set of filters ($BVr'i'$) from those used for GRB 050502a (Guidorzi et al. 2005a). The motivation for changing and optimizing the filter choice (post May 16) was threefold: (1) the greater sensitivity at g' band, (2) the small separation between B and V filter central wavelengths (444.8 and 550.5 Å, respectively), and (3) the recognized need for denser sampling of the light curves at early times.

6.2. Polarimetry Mode (PM)

A key unsolved problem in the astrophysics of GRBs is the geometry of the ejecta and the role of magnetic fields. Direct measurements of polarization at *early times* provide stringent constraints on current jet and internal shock models. As described in § 2, we will have unique access to a simple optical polarimeter, RINGO, on the LT from 2006. Polarimetry mode (PM) will be triggered following the identification by LT-TRAP of a candidate OT with $r' < 15$ mag and high significance, and will consist of an automatic series of polarimetric exposures taken with RINGO, with increasing exposure times: 30, 60, 120, 240 s, etc. These exposures will not be reduced and analyzed in real time, but postprocessing will extract the r' band light curve and any polarization evolution of the OT. Although less sensitive than RATCam, RINGO will detect polarization to the level of a few percent in $r' \lesssim 15$ mag OTs in a 30 s exposure. In combination with the initial polarimetric exposure that will be obtained immediately before the DM begins, this mode aims to measure the polarization properties from the first minutes after the burst.

6.3. Spectroscopy Mode (SM)

Following commissioning of FRODOSpec (2007), the identification of a candidate OT with $r' < 15$ mag and high significance will result in the triggering of an automatic spectroscopic observation. The goal of the initial spectroscopic observations will be to obtain an early redshift estimate, while subsequent spectra taken during the first hour will provide valuable information on the time evolution of the GRB environment and light curve. Short-exposure r' images will be interspersed with spectroscopic observations to ensure that the OT has not faded below the sensitivity limit of the spectrograph. In the case of a rapidly fading OT, the observing mode will revert to MCIM after the initial spectrum has been obtained.

6.4. RIZ Mode (RIZM)

When the DM does not identify an OT candidate, the GRB TOCA invokes the "RIZ mode." This consists of a sequence of 2 minute exposure r', i', and z' images: first, one r', one i', and one z', then two r', followed by two i' and two z', then three r' followed by three i' and three z', and so on. Prior to 2005 November, this mode consisted of $r'i'$ cycles only; we have subsequently adapted this mode to include additional z' exposures, which are inserted at the end of each $r'i'$ cycle to enable identification of possible higher redshift bursts ($z \lesssim 6$) that may be faint in r' but brighter in z'.

This mode is designed to be sensitive to possible faint optical afterglows (whether intrinsically faint or at higher redshift), allowing r', i', and z' band light curves to be constructed when an OT is detectable in longer exposures but is too faint to have been automatically identified by the DM, or to provide deep upper limits at early time when no OT is present. Under average conditions (i.e., seeing of ~1″, 2 minute exposure), limiting magnitudes are around $r' \sim 21$–22, $i' \sim 20$–21, and $z' \sim 20$.

7. LT-TRAP DEPLOYED ON OTHER FACILITIES

The LT is the prime member of the global 2 m robotic telescopes network called RoboNet-1.0.[9] This network includes two other facilities: the Faulkes Telescope North (FTN), located in Maui, Hawaii, and the Faulkes Telescope South (FTS), in Siding Spring, Australia, both mainly supported by the Dill Faulkes Educational Trust and intended for use by UK schools and various scientific observing programs. All three telescopes are operated remotely through the Telescope Management Centre at Liverpool JMU, and when fully commissioned, will all operate in fully robotic mode. Under the RoboNet-1.0 project,

[9] See http://www.astro.livjm.ac.uk/RoboNet.

comprising a consortium of 10 UK universities funded by the UK Particle Physics and Astronomy Research Council (PPARC), a fraction of time on the two FTs is reserved for post–first-hour GRB follow-up by consortium members (see Gomboc et al. [2005b, 2005c] for details).

Following the successful operation of LT-TRAP on the LT, it was deployed on the Faulkes Telescopes, with a slightly modified choice of observing mode after the OT identification stage (see Fig. 2). The FTS is currently undergoing commissioning so is not yet available robotically. The FTN is fully robotic and has performed a number of follow-up observations minutes after a GRB. For this reason, hereafter we limit our discussion to the FTN. The rapid (<1 hr) robotic follow-up observation of GRBs on the FTN is a collaborative project between LJMU and the University of Leicester.

The optical filters available on the FT are different from those on the LT: Bessell *BVR*, Sloan i', neutral *U*, O III, and Hα. The DM consists of only one set of three 10 s images in *R*. Regardless of the results of the DM, three more 10 s images are acquired in filters *B*, *V*, and i' (in that order). In the case of identification of an OT candidate with $R < 15$, the GRB TOCA will trigger a spectroscopic observation. As in the case of the LT, the threshold on the confidence level for an OT candidate to be considered a good candidate is currently set to 0.7. The logic of the selection of the OT candidate is exactly the same as it is for the LT (§ 5.2). Presently, regardless of the possible identification of an OT candidate with $R > 15$ and a confidence level >0.7 from the DM, the GRB TOCA triggers a sequence of multicolor observations, according to the following scheme: cycles of BRi' observations with increasing exposure times: 30 s (once), 60 s (once), then continuous switching between 120 and 180 s exposures, in order to limit the effects of tracking problems.

7.1. Estimation of the LT-TRAP Reliability

Although the number of GRBs observed so far is still small, we have attempted to estimate the reliability of the OT candidates automatically identified by the LT-TRAP as follows. For each of the GRBs followed up robotically within minutes, we counted the OT candidates as identified as a function of their confidence level. When the confidence level is above the threshold (currently set to 0.7), the OT is taken to be a true OT candidate (TOC), otherwise it is a fake OT candidate (FOC). When a true afterglow is present, we call it a true OT (TO); similarly, if any non-GRB source that could mimic a GRB afterglow is present, we call it a fake OT (FO). Let p_T be the probability that a TO is automatically identified as a TOC. The closer p_T is to 1, the better the LT-TRAP's capability of identifying genuine GRB afterglows. Likewise, let p_F be the probability that a FO is automatically identified as a FOC. The closer p_F is to 1, the better the LT-TRAP's capability of rejecting fake GRB afterglows. In practice, we do know that p_T and p_F are somehow correlated: a low threshold on the confidence level would increase p_T but also decrease p_F. The opposite is true for a high value of the same threshold. So far, the current value (0.7) has turned out to be a good trade-off. However, as a first approximation we treat them as unrelated, and eventually we discuss the opposite case of total correlation. Let n_T and m_T be the total number of TOs observed and the total number of TOs identified as TOCs, respectively. Likewise, let n_F and m_F be the total number of FOs observed and the total number of FOs identified as FOCs, respectively. The probability $P_T(n_T, m_T|p_T)$ [$P_F(n_F, m_F|p_F)$] of identifying m_T (m_F) TOCs (FOCs) out of n_T TOs (n_F FOs), given p_T (p_F), is given by the binomial distribution (under the sensible assumption that different GRBs are independent from each other):

$$P_i(n_i, m_i|p_i) = \binom{n_i}{m_i} p_i^{m_i}(1 - p_i)^{n_i - m_i} \quad (i = T, F). \qquad (1)$$

We do not know either p_T or p_F, but so far we have counted the following: $n_T = 2$, $m_T = 2$; $n_F = 15$, and $m_F = 13$ (in fact, LT-TRAP has so far correctly identified both $r' < 19$ OTs and failed to reject 2 out of 15 fake OTs). From the Bayes theorem, we derive the probability $P_i(p_i|n_i, m_i)$ to have p_i, given n_i and m_i:

$$P_i(p_i|n_i, m_i) = \frac{P_i(n_i, m_i|p_i)\, P(p_i)}{P(n_i, m_i)} \quad (i = T, F). \qquad (2)$$

We then apply the maximum likelihood method and find the value for p_i that maximizes $P_i(p_i|n_i, m_i)$. To this end, the denominator of equation (2) can be ignored. Concerning the knowledge of the prior $P(p_i)$, as a first guess in both cases, we can assume the simple case of a uniform distribution. We then refine it thanks to the information derived from our tests, according to which a sensible approximation is given by a truncated normal distribution centered on 0.8 and σ of 0.3. However, it must be pointed out that the prior strongly depends on the kind of afterglow population one considers. For this reason, we consider these two opposite cases of uniform and truncated normal distributions. When a uniform prior is assumed, the best value is straightforwardly given by $p_i = m_i/n_i$: $p_T = 2/2 = 1$ and $p_F = 13/15 \simeq 0.87$. When we assume a more refined prior [i.e., $P(p_i) \sim N(0.8, 0.3)$], the best values are $p_T \simeq 0.98$ (Fig. 3, *solid line*) and $p_F \simeq 0.86$. Eventually, we can provide confidence intervals on both p_T and p_F at given levels from the distributions obtained with the truncated normal priors: $p_T = 0.98^{+0.02}_{-0.16}$ and $p_F = 0.86^{+0.05}_{-0.06}$ (50% confidence level [CL]), $p_T = 0.98^{+0.02}_{-0.42}$ and $p_F = 0.86^{+0.10}_{-0.17}$ (90% CL).

If we take into account the correlation between p_T and p_F, the total probability of equation (2) is replaced by the more general one:

$$P_{T,F}(p_T, p_F|n_T, m_T, n_F, m_F) = \frac{P_T(n_T, m_T|p_T)\, P_F(n_F, m_F|p_F)\, P(p_T, p_F)}{P_T(n_T, m_T, n_F, m_F)} \qquad (3)$$

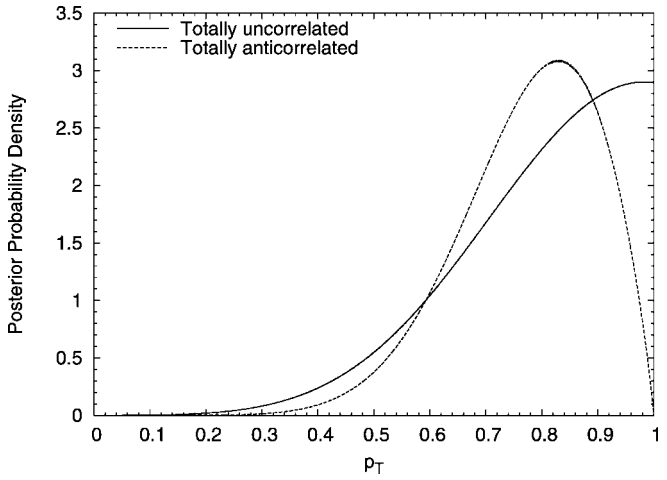

FIG. 3.—Probability density function of p_T, assuming a truncated normal prior, $N(0.8, 0.3)$, in two cases: p_T and p_F uncorrelated (*solid line*) and totally correlated (*dashed line*; see text).

At this stage, it is difficult to model the anticorrelation between p_T and p_F in the bivariate prior $P(p_T, p_F)$, particularly for the small sample of GRBs so far collected. We then studied the opposite case of a total anticorrelation between the two variables, in which p_F is completely determined by the value of p_T, by solving equation (4):

$$\int_{p_F}^{1} P_F(p'|n_F, m_F)\, dp' = \int_{0}^{p_T} P_T(p'|n_T, m_T)\, dp', \qquad (4)$$

where $P_i(p'|n_i, m_i)$ is the same expression derived in equation (2), assuming truncated normal priors. The meaning of equation (4) is that for each value p'_T, p'_F is determined so that the probability that $p_F > p'_F$ is equal to the probability that $p_T < p'_T$; it is straightforward to verify that the greater p'_F the smaller p'_T, and vice versa. This is just one sensible assumption of total anticorrelation among other possible alternative assumptions. Figure 3 shows the probability density for p_T derived in this case of total anticorrelation (*dashed line*). The best values for p_T and p_F and their confidence intervals derived in this case (truncated normal priors) are as follows: $p_T = 0.83^{+0.08}_{-0.09}$ and $p_F = 0.83^{+0.04}_{-0.05}$ (50% CL), $p_T = 0.83^{+0.14}_{-0.24}$ and $p_F = 0.83^{+0.09}_{-0.24}$ (90% CL).

Remarkably, in spite of the opposite cases of variables p_T and p_F being either totally unrelated or totally anticorrelated, the results seem to give consistent confidence intervals, as shown by Figure 3. The wide confidence interval of p_T is understandably due to the low number of TOs observed so far, rather than the limits of the LT-TRAP. We expect to give more precise estimates of both probabilities as soon as the sample of detected GRB afterglows is more numerous.

8. SOME RESULTS AND FUTURE PLANS

To date (2005 October), over a period of 2 months, the LT followed up six GRBs in a fully automated fashion using the real-time pipeline, and the FTN followed up five more. For each of these 11 follow-up observations, Table 4 reports the start time from the GRB trigger, the filters used, the number of frames acquired, and the GCN Circulars issued by the LT/FTN collaboration reporting on the corresponding LT/FTN observations. The most successful case so far is represented by the automatic detection of the afterglow of GRB 050502a (Gomboc et al. 2005a), followed by the acquisition of the first early (<1 hr) multicolor light curve (Guidorzi et al. 2005a). This latter case is also notable for longer term follow-up using the RoboNet-1.0 network. Another case of prompt detection is GRB 050713a (Monfardini et al. 2005a), although in this case the afterglow was not identified automatically, because of the poor quality of the images affected by the presence of a $V \sim 6$ star in the field, but recognized afterward by visual inspection. The power and robustness of the LT-TRAP is illustrated in the case of GRB 050730 (Gomboc et al. 2005d): this GRB occurred before

TABLE 4
RESULTS OF THE ROBOTIC FOLLOW-UP OBSERVATIONS WITH LIVERPOOL AND FAULKES NORTH TELESCOPES (2005 OCTOBER)

GRB	Telescope	Spacecraft	Filters	Start[a] (minutes)	Result	Frames	LT/FTN GCN Circulars
050412	FTN	*Swift*	*BVRi′*	2.5	$R > 18.7$	23	None
050502a	LT	*INTEGRAL*	*BVr′i′*	3.1	$r' \sim 15.8$	25	3325
050504	FTN	*INTEGRAL*	*BVRi′*	3.7	$R > 19$	38	3351
050520	LT	*INTEGRAL*	*r′i′*	4.5	$r' > 16.6$	18	3437
050528	LT	*Swift*	*r′i′*	2.5	$r' > 17.2$	36	3497
050713a	LT	*Swift*	*r′*	2.4	$r' \sim 19.2$	3	3588
050713b	FTN	*Swift*	*R*	3.3	$R > 18.2$	6	3592
050716	FTN	*Swift*	*BVRi′*	3.8	$R > 19.8$	20	3625
050730	LT	*Swift*	*r′i′*	50	$r' \sim 17.3$	36	3706
050904	LT	*Swift*	*r′i′*	3.8	[b]	31	None
050925	FTN	*Swift*	*BVRi′*	3.3	$R > 19.0$	12	4035

[a] This corresponds to the time delay with respect to the GRB trigger time.

[b] The afterglow of GRB 050904 (Haislip et al. 2005) was found to lie outside the field of view of the LT (3′.9 away from the BAT position).

twilight at the LT site, so was triggered manually, and although the OT was not recognized during the DM because of the high sky background due to the sky not yet being completely dark, it was automatically identified in the subsequent RI mode as an unknown fading source of $r' = 17.3$ at $t \sim 50$ minutes after the GRB. In the other cases, the combination of sensitivity and rapid response made it possible to derive deep upper limits, as in the cases of GRB 050504, with $R > 19$ (Monfardini et al. 2005b), and GRB 050716, with $R > 19.8$ (Guidorzi et al. 2005b), 3–4 minutes after the GRB trigger time.

In the future, we plan to refine the strategy when an OT candidate with $R > 15$ and a confidence level >0.7 is found from the DM; in particular, exposure times will be tuned dynamically, on the basis of the estimated magnitude of the best OT candidate. Automatic polarimetry, near-infrared, and spectroscopy follow-up modes will be implemented on the LT following completion of instrument commissioning.

C. G. and A. G. acknowledge their Marie Curie Fellowships from the European Commission. C. G. M. acknowledges financial support from the Royal Society. A. M. acknowledges financial support from the UK PPARC. M. F. B. is supported by a PPARC Senior Fellowship. The Liverpool Telescope is operated on the island of La Palma by Liverpool John Moores University at the Observatorio del Roque de los Muchachos of the Instituto de Astrofísica de Canarias. The Faulkes Telescope North is operated with support from the Dill Faulkes Educational Trust.

REFERENCES

Bertin, E., 1996, A&AS, 117, 393
Clarke, D., & Neumayer, D. 2002, A&A, 383, 360
Fraser, S. N., & Steele, I. A. 2002, Proc. SPIE, 4848, 443
———. 2004, Proc. SPIE, 5493, 331
Gomboc, A., Steele, I. A., Monfardini, A., Mottram, C. J., Guidorzi, C., Bode, M. F., & Mundell, C. G. 2005a, GCN Circ. 3325
Gomboc, A., et al. 2005b, in AIP Conf. Proc. 797, Interacting Binaries: Accretion, Evolution, and Outcomes, ed. L. Antonelli et al. (New York: AIP), 181
———. 2005c, Nuovo Cimento, 28, 723
———. 2005d, GCN Circ. 3706
Greisen, E. W., & Calabretta, M. R. 2002, A&A, 395, 1061
Guidorzi, C., et al. 2005a, ApJ, 630, L121
Guidorzi, C., et al. 2005b, GCN Circ. 3625
Haislip, J., Reichart, D.E., Cypriano, E., Pizzaro, S., LaCluyzé, A., Rhoads, J., & Figuerêdo, E. 2005, GCN Circ. 3913
Mink, D. J. 2002, in ASP Conf. Proc. 281, Astronomical Data Analysis Software and Systems XI, ed. D. A. Bohlender et al. (San Francisco: ASP), 169
Monet, D. G., et al. 2003, AJ, 125, 984
Monfardini, A., Guidorzi, C., Steele, I. A., Mottram, C. J., Carter, D., Gomboc, A., Mundell, C., & Bode, M. 2005b, GCN Circ. 3351
Monfardini, A., et al. 2005a, GCN Circ. 3588
Rykoff, E. S., et al. 2004, ApJ, 601, 1013
Schlegel, D. J., Finkbeiner, D. P., & Davis, M. 1998, ApJ, 500, 525
Steele, I. A., & Carter, D. 1997, Proc. SPIE, 3112, 223
Steele, I. A., et al. 2004, Proc. SPIE, 5489, 679
van Paradijs, J., et al., 1997, Nature, 386, 686
Vestrand, W. T., et al. 2005, Nature, 435, 178